Magnetic Resonance in Medicine 43:383–392 (2000)

Functional MRI of Calcium-Dependent Synaptic Activity: Cross Correlation With CBF and BOLD Measurements

Timothy Q. Duong, Afonso C. Silva, Sang-Pil Lee, and Seong-Gi Kim*

Spatial specificities of the calcium-dependent synaptic activity, hemodynamic-based blood oxygenation level-dependent (BOLD) and cerebral blood flow (CBF) fMRI were quantitatively compared in the same animals. Calcium-dependent synaptic activity was imaged by exploiting the manganese ion (Mn^{++}) as a calcium analog and an MRI contrast agent at 9.4 T. Following forepaw stimulation in α-chloralose anesthetized rat, water T_1 of the contralateral forepaw somatosensory cortex (SI) was focally and markedly reduced from 1.99 ± 0.03 sec to 1.30 ± 0.18 sec (mean ± SD, *N* = 7), resulting from the preferential intracellular Mn^{++} accumulation. Based on an in vitro calibration, the estimated contralateral somatosensory cortex [Mn^{++}] was ~100μM, which was 2–5-fold higher than the neighboring tissue and the ipsilateral SI. Regions with the highest calcium activities were localized around cortical layer IV. Stimulus-induced BOLD and CBF changes were 3.4 ± 1.6% and 98 ± 33%, respectively. The T_1 synaptic activity maps extended along the cortex, whereas the hemodynamic-based activation maps extended radially along the vessels. Spatial overlaps among the synaptic activity, BOLD, and CBF activation maps showed excellent co-registrations. The center-of-mass offsets between any two activation maps were less than 200 μm, suggesting that hemodynamic-based fMRI techniques (at least at high field) can be used to accurately map the spatial loci of synaptic activity. Magn Reson Med 43:383–392, 2000. © 2000 Wiley-Liss, Inc.

Key words: electrical activity; forepaw somatosensory stimulation; cerebral blood flow; hemodynamic response

In mammalian brain, neuronal activity involves a cascade of calcium (Ca^{++}) influx from the extracellular into the intracellular space. Upon depolarization at its postsynaptic terminals, neuron triggers an instantaneous rise in the intracellular calcium concentration by opening voltage-gated and/or ligand-gated calcium channels in the presynaptic terminals (1). This subsequently triggers neurotransmitter releases at the postsynaptic clefts. Consequently, calcium is one of the most robust indicators for neuronal activities in brain.

In vitro studies of intracellular calcium accumulation had been reported using a variety of techniques. In particular, the use of calcium-sensitive fluorescent dyes (2,3) had revealed critical role of calcium activities in developmental (3) and memory functions (4). However, detecting intracellular calcium accumulation in vivo noninvasively and with high spatial resolution has proven to be difficult. By using two-photon microscopy (2), in vivo measurement of calcium activity had been reported. Unfortunately, the use of two-photon microscopy in vivo is hampered by its limited field of view and invasiveness.

Recently, Lin and Koretsky (5,6) introduced a technique that can directly "visualize" calcium-dependent synaptic activity by MRI using a calcium analog, manganese ion (Mn^{++}), as an MRI contrast agent. Manganese is known to enter the intracellular space via voltage-gated calcium channels (7–9) following the trigger of an action potential (10). Manganese is also known to mimic the physiological role of calcium in supporting increased neural transmitter release from depolarized nerve ending (7). The influxed Mn^{++} is trapped in the intracellular space with an intracellular half-life of 2–3 months (11,12). The preferential accumulation of paramagnetic Mn^{++} in actively firing neurons associated with increased synaptic activity results in marked shortening of regional water proton T_1, which can be detected by using ^1H_2O T_1-weighted and T_1-map imaging. By using T_1-weighted imaging, Lin and Koretsky demonstrated that Mn^{++}-induced T_1-weighted contrast following glutamate and somatosensory stimulation could be detected (5,6). Therefore, the dual role of Mn^{++} as a calcium analog and an MRI contrast agent gives rise to an opportunity to directly image neuronal processes in vivo.

This Mn^{++} technique, however, remains to be vigorously cross-validated. The goal of this study, therefore, was to compare the calcium-dependent synaptic activity measurements with the commonly used blood oxygenation level-dependent (BOLD) (13) and cerebral blood flow (CBF) (14) fMRI techniques. Specifically, we demonstrated that calcium-dependent synaptic activity can be measured by using ^1H quantitative T_1 imaging, and compared quantitatively the spatial registrations between calcium-dependent synaptic activity and hemodynamic responses following neural stimulation. The well-established somatosensory (forepaw) stimulation paradigm in α-chloralose anesthetized rats (15–20) was employed. Synaptic activity and hemodynamic responses following forepaw stimulation were measured in the same animal on a 9.4 T MRI scanner. Calcium-dependent synaptic activity was measured using T_1 echo-planar imaging (EPI) following systemic infusion of the manganese ion. BOLD and CBF responses were simultaneously measured in the same animal. The spatial registrations among the T_1- (synaptic activity), BOLD-, and CBF-activation maps were quantitatively compared. Further, we also extended the Mn^{++} technique by introducing an improved infusion protocol and surgical procedure, which yielded better tissue (in contrast to vascular) specificity and made possible the simultaneous CBF measurement using the continuous arterial spin-labeling method.

Center for Magnetic Resonance Research, Department of Radiology, University of Minnesota School of Medicine, Minneapolis, Minnesota.

Grant sponsor: NIH; Grant numbers: RR08079; NS38195; Grant sponsors: Keck Foundation; Whitaker Foundation; Grant sponsor: NIH fellowship (TQD); Grant number: NS10930.

*Correspondence to: Seong-Gi Kim, Ph.D., Center for Magnetic Resonance Research, University of Minnesota School of Medicine, Radiology, 2021 Sixth Street SE, Minneapolis, MN 55455. E-mail: kim@cmrr.umn.edu

Received 21 July 1999; revised 8 October 1999; accepted 2 November 1999.

METHODS

Animal Surgery

Seven male Sprague Dawley rats (230–270 g) were anesthetized with 1–2% (v/v) halothane in a mixture of O_2:N_2O gases during surgery. Following oral intubation, one femoral artery and two femoral veins were catheterized with PE-50 tubing (polyethylene tubing, Fisher Scientific) for physiological monitoring, blood gas sampling, and chemical administration. For delivering mannitol to break the blood-brain barrier (BBB), the right external carotid artery (ECA) was used to gain access to the internal carotid artery without interrupting blood flow to the brain during the MR experiment. The common carotid and the internal carotid artery around the ECA bifurcation were temporally ligated. The ECA was permanently ligated proximally and distally. It was then severed and flipped 180° such that it lay parallel to the common carotid artery. The ECA was then catheterized with a PE-50 tubing. Mannitol could later be administered from the severed ECA toward the internal carotid artery and the brain but not toward the heart. This surgical procedure is similar to that used for intraluminal occlusion of the middle cerebral artery in rat stroke model.

Blood gas was sampled every 0.5–2.0 hr and maintained at the physiological levels (pH = 7.35–7.45, pCO_2 = 30–40 mm Hg, pO_2 = 120–200 mm Hg, and mean arterial blood pressure = 90–130 mm Hg). The animal's rectal temperature was maintained at 37 ± 1°C. Blood oxygen saturation and heart rate was also monitored using an oximeter (Nonin Medical Inc., MN) with the fiberoptic probe wrapped around the tail of the animal.

Administration of Agents

After surgery, anesthesia was switched from halothane to α-chloralose (an initial intravenous dose of 80 mg/kg, followed by a continuous intravenous infusion of a 5 mg/ml α-chloralose solution at 2–3 ml/hr). Continuous α-chloralose was infused via one of the two catheterized femoral veins. The other PE-50 femoral venous line was filled with $MnCl_2$ before placing the animal in the magnet. After approximately 2–3 sets of BOLD/CBF and baseline T_1 measurements, a 120-mM $MnCl_2$ solution (Sigma, St. Louis, MO) was infused at a rate of 2 ml/hr for ~20–30 min while the animal was inside the magnet. Approximately 10 min following the initiation of $MnCl_2$ infusion, the initially saline-filled PE-50 line, catheterized to the ECA, was slowly displaced by mannitol solution over ~1 min immediately prior to mannitol administration. A bolus of 25 % D-mannitol (5 mg/kg, Sigma) was administered steadily over ~30 sec via the severed ECA to break the BBB.

Forepaw Stimulation

Two needle electrodes were inserted under the skin of the animal's left forepaw between digits 2 and 5 for forepaw stimulation. Stimulation employed a 1.5 mA current with 0.3 msec pulse duration at 3 Hz, which were optimized to induce a strong CBF response without observable changes in mean arterial blood pressure (see Ref. 22). For BOLD/CBF measurements, the stimulation paradigm was 2 min OFF, 1 min ON, and 2 min OFF. For T_1 measurements, the stimulation paradigm was 10 min OFF and 10 min ON and repeated at least three times. Typically, only T_1 maps obtained from the third or fourth stimulation block was used for further analysis.

MR Experiments

MR experiments were performed on a 9.4 T/31-cm horizontal magnet (Magnex, UK) equipped with a ^{Unity}INOVA console (Varian, CA), and a 30 G/cm magnetic field gradient insert (ID = 11 cm, 300 μs risetime; Magnex, UK). The animal was secured in a head-holder with ear and bite bars to reduce motion artifacts. A surface coil of 1.2-cm diameter was positioned on top of the rat head and the animal was placed on a cradle, which has a built-in butterfly spin-labeling coil of 0.5-cm diameter at the animal's neck position. The distance between the imaging and the spin-labeling coils was typically 1.8 cm. Coil-to-coil electromagnetic decoupling was optimized by orthogonality to better than 20 dB isolation.

Exploratory multi-slice BOLD experiments using single-shot, gradient-echo (GE) EPI were performed to select a single, 2 mm coronal image slice (that covered essentially the entire activated forepaw somatosensory cortex) for subsequent MR measurements. T_1 baseline and BOLD/CBF measurements were made. Mn^{++} and mannitol were administered. T_1 measurements were made. In some cases, BOLD/CBF measurements were again made. However, only the BOLD/CBF measurements made before the Mn^{++} administration were used for further analysis.

Synaptic Activity (T_1) Measurement

T_1 measurements were made using two-segment, spin-echo (SE), inversion-recovery EPI without signal averaging. The spin-echo portion consisted of a non-spatially selective, adiabatic half-passage pulse (2 msec) for excitation and two spatially selective, full-passage pulses (2 msec) for refocusing (21). A nonspatially selective, adiabatic full-passage pulse (8 msec) was used for the spin inversion. The imaging parameters were: data matrix = 128 × 64, FOV = 3.0 cm (readout) × 1.5 cm (phase encoding), slice thickness = 2 mm, TR = 8 sec, TE = 10 msec, and 9 variable inversion delays (0.05, 0.1, 0.25, 0.5, 1, 2, 4, 7, and 11 sec). The temporal resolution of the T_1 measurement was ~10 min.

Combined BOLD/CBF Measurement

Combined BOLD and CBF measurements were made using single-shot, GE EPI without signal averaging. CBF measurements were made using the continuous arterial spin-labeling perfusion technique (19,20). Paired images were acquired alternately—one with arterial spin labeling and the other without spin labeling (control). The MR imaging parameters were: data matrix = 64 × 32, FOV = 3.0 cm (readout) × 1.5 cm (phase encoding), slice thickness = 2 mm, TE = 10 msec, and TR = 3.03 sec. The continuous arterial spin labeling employed a 3-sec square radiofrequency pulse to the labeling coil in the presence of 1.0 G/cm gradient along the flow direction such that the condition of adiabatic inversion was satisfied (14). The sign of the frequency offset was switched for control (nonlabeled)

images. Fifty pairs of images were acquired, yielding a temporal resolution of ~5 min.

Data Analysis

Image analysis employed the STIMULATE software (22) and codes written in PV-WAVE (Visual Numeric Inc., CO). Images are displayed in radiological convention (right hemisphere is on the left-hand side of the displayed image). All statistical tests employed the Student paired *t*-test and all reported values were in mean ± SD and unless otherwise specified.

Constructing Synaptic T_1 Activation Maps

T_1 maps were calculated on a pixel-by-pixel basis (23). For consistency in cross-subject and cross-modality comparison, the T_1-activation map of the Mn^{++}-infused rat brain was constructed by setting an upper T_1 threshold on the entire contralateral cortex such that ~50 activated pixels were obtained. The maximum T_1 value of the ~50 pixels was at least 1–2 SD smaller than the average T_1 value of the entire contralateral cortex. The area covered by 50 pixels (2.7 mm^2) accurately represented the area of the forepaw somatosensory cortex, as reported by a histological study of 2.2 mm^2 (24), a single-unit recording of 2.54 mm^2 (25), a fluorescence study of 3.1 mm^2 (25), and a rat brain atlas of ~3.0 mm^2 (determined by cut-and-weigh method) (26).

Constructing BOLD/CBF Activation Maps

BOLD and CBF data were zero-filled from a data matrix of 64×32 to 128×64. BOLD images were obtained from the nonlabeled images of the CBF measurements. CBF images were obtained by pair-wise pixel-by-pixel subtraction of the labeled from nonlabeled images. CBF map with image intensity (S_{CBF}) in units of ml/gram tissue/min was calculated using (27),

$$S_{CBF} = \frac{\lambda}{T_1} \frac{S_C - S_L}{S_L + (2\alpha - 1)S_C} \quad [1]$$

where S_C and S_L are signal intensities of the control and labeled images, respectively. λ is the water brain-blood partition coefficient, T_1 is that of tissue, and α is the arterial spin-labeling efficiency. The values of λ, T_1, and α were 0.9 (28), 1.9 sec (29), and 0.81 (20), respectively.

Cross-correlation (CC) BOLD and CBF activation maps with 95% confidence threshold (corresponding to a CC value of 0.3; 30) and with ~50 pixels having the highest CC coefficients were computed. Percent-change BOLD and CBF activation maps were also computed.

Calculating Spatial Registration of Activation Maps

For quantitative comparison across different imaging modalities of different CNR, activation maps with fixed number (~50) of pixels with the highest statistical significance were used. Two approaches were considered. In the first approach, the spatial overlaps of ~50 activated pixels between any two types of activation maps were determined. In the second approach, the spatial loci of the CBF-, BOLD- and T_1-activation maps were obtained by calculating the centers of mass (COM) of the activation maps. The COM of the BOLD- and CBF-activation maps were weighted by the t-values (which were converted from the CC values; 31), and those of the T_1 activation maps were weighted by $\Delta(1/T_1)$. Note that *t*-value was chosen for COM calculation because *t*-value is based on linear scale while cc value is not. The relative COM offsets among the CBF-, BOLD- and T_1-activation maps were also determined.

RESULTS

Mn^{++} Calibration

A standard in vitro calibration relating water $1/T_1$ to $[Mn^{++}]$ was made in saline phantoms containing 0.0, 0.4, 0.6, and 1.2 mM of $MnCl_2$. The calibration at 37.0 ± 0.5°C yielded,

$$\frac{1}{T_1([Mn^{++}])} = \frac{1}{T_1([Mn^{++}] = 0)} + 2.742 \cdot [Mn^{++}] \quad [2]$$

where $T_1([Mn^{++}])$ indicates the T_1 in seconds as a function of Mn^{++} concentration in mM. The $T_1([Mn^{++}] = 0)$ indicates T_1 at $[Mn^{++}] = 0$ and has a value of 2.98 sec. The tissue T_1 before Mn^{++} infusion was used in the place of $T_1([Mn^{++}] = 0)$ to estimate the in vivo $[Mn^{++}]$.

Mn^{++}-Induced T_1 Response

Following systemic Mn^{++} infusion, little or no changes in mean blood pressure and/or heart rate were observed. Subsequent mannitol administration to break the BBB caused transient decreases in mean blood pressure and heart rate in most cases. In some cases, the decreases in mean blood pressure and heart rate remained depressed ~20 mm Hg and 30 bpm, respectively, below normal. In a separate set of experiments in which only mannitol was administered to break the BBB, no significant changes in mean blood pressure and/or heart rate were observed (data not shown). The slight deviations from the recorded physiological parameters thus appeared to be a result of combined Mn^{++} and mannitol administration. After Mn^{++} and mannitol administration, BOLD and CBF responses were also observed ($N = 3$, data not shown). However, BOLD and CBF contrasts were reduced. This was because the paramagnetic Mn^{++} reduced water T_2^* and T_1, and thus, resulted in a loss of stimulus-induced BOLD and CBF contrast, respectively. Taken together, these data indicated that the cerebrovascular hemeostasis was not significantly perturbed following Mn^{++}/mannitol administration.

Figure 1 shows quantitative T_1 maps of two representative animals before (A, B), and after Mn^{++}/mannitol administration and forepaw stimulation (C, D). The image intensities of the T_1 maps indicate true T_1 values. Before Mn^{++} infusion, the T_1-maps were relatively uniform with the forepaw cortex T_1 values of ~2.0 sec. After Mn^{++}/mannitol administration and stimulation, the overall contralateral hemisphere (left side of the displayed image) in which mannitol was directly administered appeared slightly and heterogeneously darkened, indicating selective Mn^{++} accumulation due to regional differences in

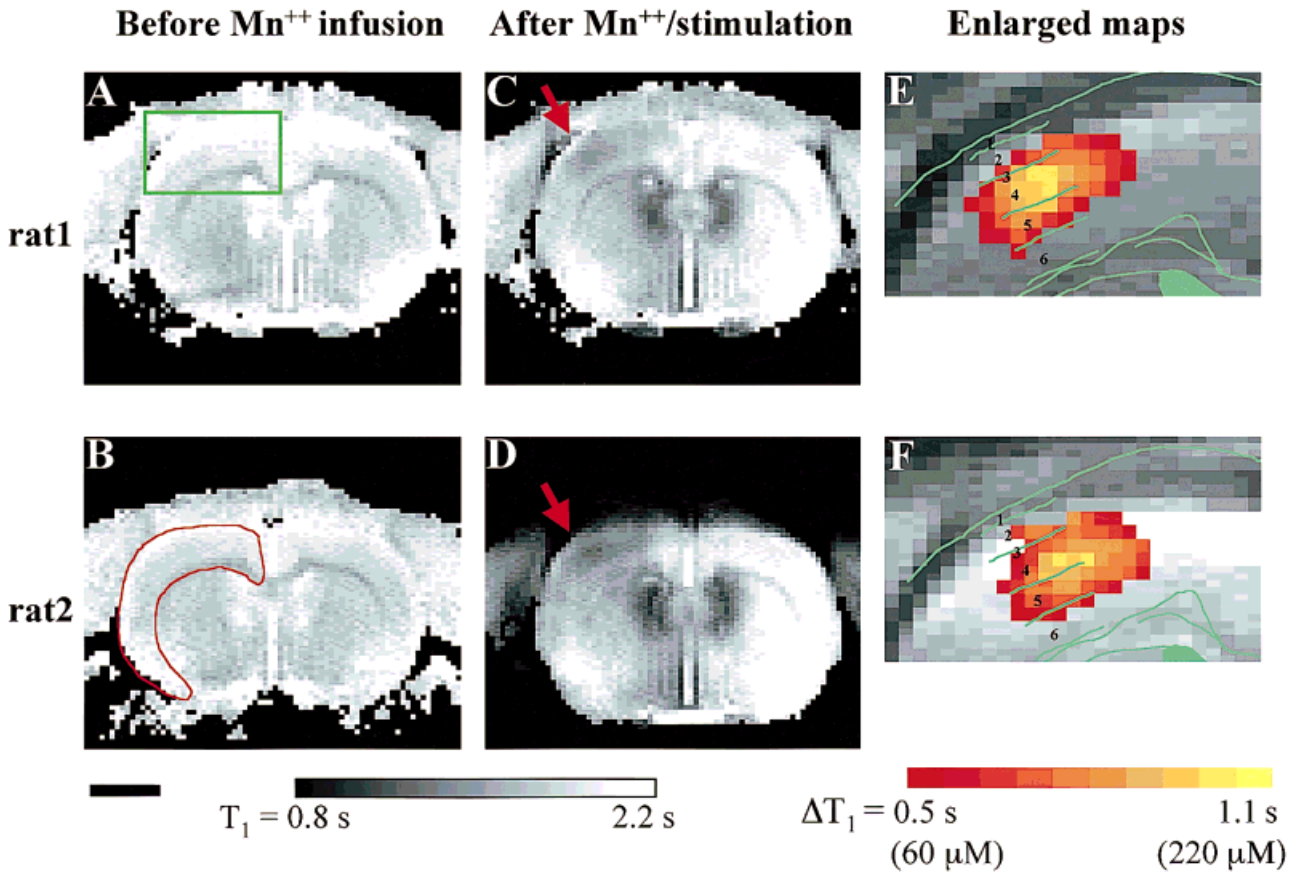

FIG. 1. T_1 maps (coronal view) before (**A**, **B**) and after Mn^{++}/mannitol administration and forepaw stimulation (**C, D**), and expanded calcium-dependent synaptic activation maps (**E**, **F**) for two representative animals. The overall right hemisphere (left side of the image) in which mannitol was directly administered appeared slightly darker than the left hemisphere. Following forepaw stimulation (**C**, **D**), the contralateral SI (indicated by the red arrows) was selective and focally darkened. The gray scale bar indicates T_1 values for panels **A**–**D**. An ROI showing the region of expansion is shown in panel **A** and an ROI outlining the entire contralateral cortex is shown in panel **B**. Panels **E** and **F** depict enlarged synaptic activity maps and cartoons showing the cortical layer information, superimposing on the corresponding anatomical images. The cartoon (26) and the anatomical image were visually matched and overlaid based on the size of the cortex. The colored bar indicates the change in T_1 values (relative to the baseline) and the corresponding [Mn^{++}]. The "hot spots" of the synaptic activity were highly localized to cortical layer IV. The scale bar is ~5 mm for panels **A**–**D**, and ~2 mm for panels **E**–**F**.

basal synaptic activity and/or BBB endothelial permeability to Mn^{++}. The ipsilateral hemisphere also appeared slightly (but less) darkened. This was because Mn^{++} also permeated the intact BBB and/or mannitol also broke the BBB of the left hemisphere to some extents via co-lateral perfusion (i.e., via the anterior communicating artery). The cerebral lateral ventricles were darkened, consistent with the high permeability of the endothelial cells underlying the choroid plexus and previous reports (5,6). Most importantly, the primary somatosensory cortex (SI) contralateral to the stimulated forepaw was focally and markedly darkened (red arrows), indicating selective Mn^{++} accumulation due to increased neuronal activity. In a separate set of experiments in which Mn^{++} and mannitol were administered without forepaw stimulation, no focal T_1 decrease in the forepaw SI was observed ($N = 3$, data not shown).

Panels E and F of Fig. 1 show synaptic activity maps (~50 pixels of the highest statistical significance) of the contralateral SI overlaid on the enlarged anatomical images, along with cartoons showing the cortical layer information. The color scale represents the difference in T_1

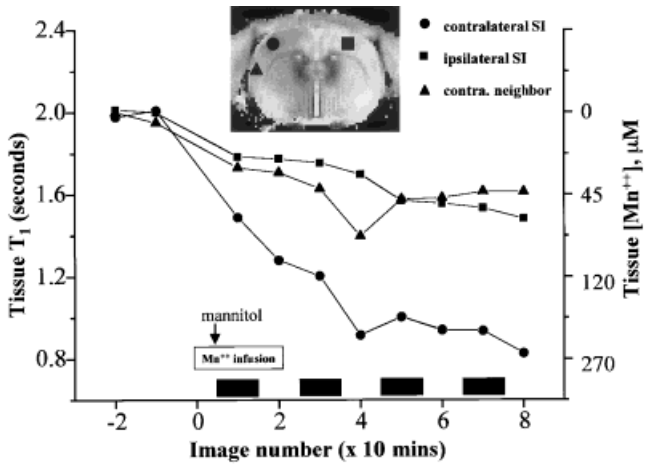

FIG. 2. T_1 and [Mn^{++}] time-courses of the contralateral SI, contralateral neighbor cortex, and the ipsilateral SI from a single animal. The ROIs and their positions used for constructing these time courses are shown in the inset. The timings for Mn^{++} and mannitol administration are also displayed. The black bars under the traces indicate the 10-min stimulation periods.

Table 1
Comparison of Regional T_1 (s) and [Mn^{++}] (μM) Prior and Following Forepaw Stimulation at 9.4 T (Mean ± SD, $n = 7$)

	Prior to Mn^{++}/mannitol administration	"Activated" contralateral SI[a]	Neighbor contralateral cortex[a]	Ipsilateral SI[a]
Rat 1	2.01	1.41	1.66	1.90
Rat 2	1.95	1.26	1.55	1.88
Rat 3	1.98	1.18	1.60	1.62
Rat 4	2.01	1.51	1.65	1.70
Rat 5	1.98	1.49	1.67	1.82
Rat 6	2.03	1.04	1.50	1.82
Rat 7	2.00	1.18	1.55	1.86
Mean ± SD[b]	1.99 ± 0.03	1.30 ± 0.18	1.60 ± 0.07	1.80 ± 0.10
[Mn^{++}], μM	0	103 ± 40	46 ± 10	20 ± 12

[a]See Fig. 2 for the ROI locations. For consistency across animals, the T_1 values of columns 3–5 were obtained from the 3rd or 4th stimulation epoch (~40–50 min) following mannitol administration.
[b]Intersubject SD of the mean. T_1 from the activated SI contralateral to the stimulated paw was statistically different from the contralateral neighbor cortex ($P < 0.0004$) and from the ipsilateral SI ($P < 0.0005$). The variance of a single pixel from baseline T_1 map was ~0.01 sec in the somatosensory cortex region.

values relative to the baseline T_1 values; a larger difference in T_1 values indicated a higher concentration of Mn^{++} accumulation, corresponding to a higher level of calcium-dependent synaptic activity. Based on these quantitative T_1 maps, regional tissue Mn^{++} concentrations were estimated via the use of the standard calibration curve (Eq. [2]). The maximum tissue [Mn^{++}] per pixel basis were <250 μM. Regions with the highest level of synaptic activity ("hot spots") were highly localized deep in the cortical layer IV of the forepaw SI.

Figure 2 shows a single-animal T_1 and [Mn^{++}] time-courses of the "activated" SI contralateral to the stimulated forepaw, the neighbor cortex contralateral to the stimulated forepaw, and the SI ipsilateral to the stimulated forepaw. T_1 values in the contralateral SI were incrementally and markedly reduced following each repeated stimulation epoch relatively to the other two regions. T_1 and [Mn^{++}] in the contralateral SI were significantly different from those in the ipsilateral SI ($P < 4 \times 10^{-6}$, paired *t*-test of the time course after mannitol administration) and contralateral neighbor cortex ($P < 3 \times 10^{-5}$). T_1 and [Mn^{++}] in the contralateral neighbor cortex and the ipsilateral SI, on the other hand, were not statistically different from each other ($P = 0.23$).

Regional T_1 values and [Mn^{++}] of the contralateral SI, ipsilateral SI, and contralateral neighbor cortex prior to and after Mn^{++} infusion/forepaw stimulation are summarized in Table 1. Prior to the Mn^{++} infusion, the average baseline T_1 of the contralateral forepaw SI was 1.99 ± 0.03 sec. Following Mn^{++}/mannitol administration and forepaw stimulation, the average T_1 value of the contralateral forepaw SI was 1.30 ± 0.18 sec (corresponding to 103 ± 40 μM [Mn^{++}]). The T_1 values of the contralateral forepaw SI were statistically different from those of the contralateral neighbor cortex (1.60 ± 0.07 sec, corresponding to 46 ± 10 μM [Mn^{++}]) and from those of the ipsilateral forepaw SI (1.80 ± 0.10 sec, corresponding to 20 ± 12 μM [Mn^{++}]). The cross-subject variations in T_1 values in Table 1 were

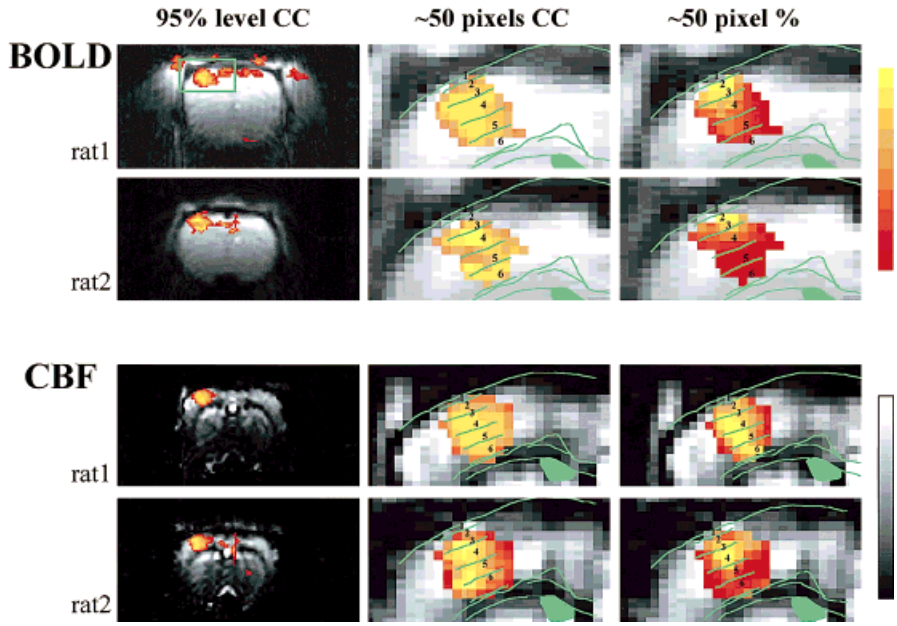

FIG. 3. Cross-correlation activation maps of the BOLD and CBF responses from the same two rats shown in Fig. 1. Cross-correlation activation maps of 95% confidence level (left column) and, ~50 pixels with the highest CC coefficients (middle column), and percent change maps of ~ 50 pixels (right column), overlaying on the corresponding anatomical and CBF images, are displayed. The gray scale bar indicates CBF values ranging from 0.1 to 1.0 ml/gram/min for the background CBF images. The colored bar indicates the cross-correlation coefficients ranging from >0.3 to 1.0 and the percent changes ranging from 1 to 5% (BOLD) and 50 to 150% (CBF). In both BOLD and CBF responses, activation in the SII cortical region was not observed, consistent with the Mn^{++} study.

Table 2
Percent Changes and CC Coefficients of BOLD and CBF Responses at 9.4 T (Mean ± SD, $n = 7$)

	BOLD		CBF		
	Mean %[a]	Mean CC[b]	Mean %[a]	Mean CC[b]	Baseline[c]
Rat 1	2.6	0.81	140	0.76	0.79
Rat 2	5.8	0.56	61	0.65	0.95
Rat 3	4.7	0.74	106	0.58	0.60
Rat 4	1.7	0.72	68	0.59	0.74
Rat 5	1.7	0.66	68	0.43	0.64
Rat 6	4.1	0.74	104	0.56	0.70
Rat 7	3.2	0.75	136	0.29	0.41
Mean ± SD[d]	3.4 ± 1.6	0.71 ± 0.08	98 ± 33	0.55 ± 0.15	0.69 ± 0.17

[a]Mean percent (%) changes of the ~50 activated pixels.
[b]Mean cross-correlation (CC) coefficients of the ~50 activated pixels.
[c]Average baseline CBF values, in unit of ml/gram tissue/min.
[d]Intersubject SD of the mean.

mainly due to the variations in tissue [Mn^{++}] that were actually achieved in the cortex across different animals. The actual tissue [Mn^{++}] depended on the intravascular [Mn^{++}], the change in BBB permeability by mannitol, and the stimulation duration, which were slightly different from animal to animal. These variations also manifested in the differences in overall T_1 maps across different animals (Fig. 1).

BOLD and CBF Responses

BOLD and CBF contrasts during forepaw stimulation were consistently observed in all animals before Mn^{++} infusion. Representative BOLD and CBF activation maps from the same two animals, respectively overlaid on the corresponding baseline anatomical and CBF images, are shown in Fig. 3. With the CC threshold set at 95% confidence level, the BOLD responses appeared diffused, extending medially and toward the dura, whereas the CBF responses appeared relatively more localized. The "hot spots" of the BOLD and CBF statistical maps were localized deep in the granular layer (i.e., layer IV) of the forepaw SI. The regions with the highest CBF percent changes (Fig. 3, third column) were also localized deep in the somatosensory cortices. On the other hand, pixels with the highest BOLD percent change were localized to the cortical surface where there were significant large vessel contributions. These observations were consistent across all seven animals.

Table 2 summarizes the mean cross-correlation coefficients and percent changes of the BOLD- and CBF-activation maps. BOLD and CBF responses increased 3.4 ± 1.6% and 98 ± 33%, respectively, during forepaw stimulation, consistent with those reported by Silva et al. (19,20) under essentially identical conditions. The baseline CBF value was 0.69 ± 0.17 ml/gram tissue/min, consistent with that measured by the iodoantipyrine autoradiographic technique of 0.72 ± 0.19 (mean ± SD, $N = 5$) (15), 0.85 ± 0.24 (mean ± SEM, $N = 5$) (29), and by the FAIR technique of 0.91 ± 0.31 (mean ± SEM, $N = 5$) (29).

Cross Comparison Among Three Imaging Modalities

The spatial overlaps among synaptic activity, BOLD, and CBF activation maps from the same two representative animals are shown in Fig. 4. In most animals, the shape of the synaptic activity maps extended along the cortex and not radially along the vessel direction, consistent with that of the electrophysiological recordings. On the other hand, most BOLD and CBF activation maps extended radially along the vessel direction. Nevertheless, the spatial overlaps among these activation maps were highly significant: 78 ± 10% between BOLD- and CBF-activation map, 61 ±

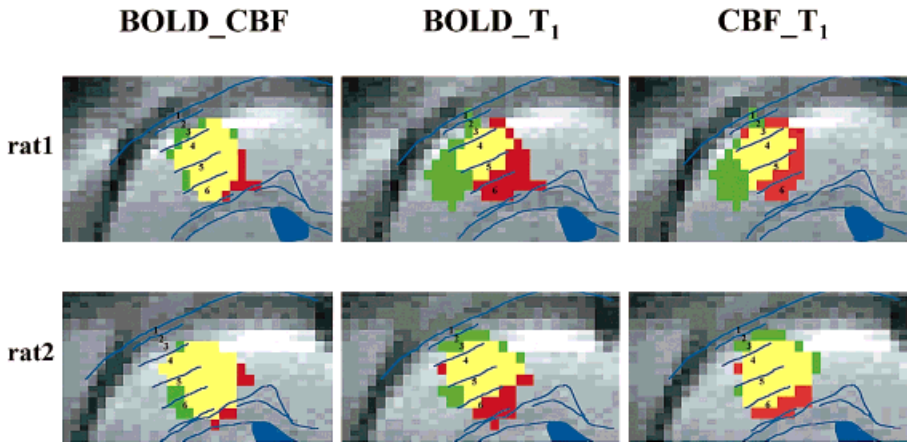

FIG. 4. Spatial overlaps of activation maps from the same two rats shown in Fig. 1. The first column shows the combined maps of BOLD (red), CBF (green), and the overlap between the two (yellow). The second column shows the combined maps of BOLD (red), T_1 (green), and the overlap between the two maps (yellow). The third column shows the combined maps of CBF (red), T_1 (green), and the overlap between the two (yellow).

Table 3
Center-of-Mass Stereotaxic Coordinates (in Unit of mm) of CBF, BOLD, Synaptic Activity (T_1) Activation Maps (Mean ± SD, $n = 7$)[a]

	Distance from midline	Distance from surface
CBF	3.47 ± 0.48	1.45 ± 0.29
BOLD	3.35 ± 0.46	1.44 ± 0.34
Synaptic activity (T_1)	3.53 ± 0.51	1.38 ± 0.28
Reference[b]	~3.50	~1.40

[a]The centers of mass between any two activation maps were not statistically different from each other ($P > 0.2$), except between BOLD and CBF in the lateral-medial direction ($P < 0.01$). The centers of mass of the BOLD activation maps were located more medial to midline than that of CBF activation maps, consistent with those reported by Silva et al. (22).
[b]Stereotaxic coordinates of the forepaw SI from a rat brain atlas (26).

11% between CBF and T_1-activation map, and 59 ± 10% between BOLD- and T_1-activation map.

The "hot spots," as indicated by the COM, of the three imaging modalities showed excellent spatial colocalization. The average COM of the CBF, BOLD, and T_1 activation maps from the midline and surface dura are summarized in Table 3. The COM coordinates were in excellent agreement with the forepaw SI stereotaxic coordinates for the rat brain atlas (26). The average COM offsets between any two activation maps, summarized in Table 4, were less than 200 μm (~1 pixel dimension).

DISCUSSION

The potential systemic toxicity of Mn^{++} is of major concern in using Mn^{++} as a tool to detect synaptic activity. After Mn^{++}/mannitol administration, little or no changes in physiological parameters were observed, consistent with previous reports (5,6). Further, our data also suggested that the cerebrovascular hemostasis was not significantly perturbed because the animal exhibited CBF and BOLD responses to forepaw stimulation following Mn^{++}/mannitol administration. In regards to potential Mn^{++} tissue toxicity and/or cytotoxicity, the average [Mn^{++}] in the forepaw SI was found to be ~100 μM, with the maximum [Mn^{++}] per pixel <250 μM. Based on the marked T_1 contrast, the intravascular Mn^{++} dosage could be reduced to minimize potential toxicity. Nevertheless, there were evidences that Mn^{++} support calcium transport at 0.3 mM concentration, whereas Mn^{++} inhibited ATP-dependent calcium transport at 1.8 mM (32). Therefore, studies from this and other laboratories suggested that the Mn^{++} dose administered herein did not significantly perturb cellular and cerebrovascular function.

Breaking the BBB appeared to be necessary to detect Mn^{++}-induced T_1 contrast (even at high field where T_1 dynamic range is relatively large). Similar experiments performed without breaking the BBB ($N = 5$, data not shown) did not show focal T_1 decrease in the contralateral cortex. This is likely due to insufficient Mn^{++} being accumulated in the forepaw cortex to yield observed contrast.

MR Imaging of Synaptic Activity

In principle, the T_1 value is a quantitative measure of [Mn^{++}]. However, in vivo Mn^{++} relaxivity may be slightly different from that in vitro due to its interaction with macromolecules in vivo. Further, intracellular water exchange lifetime is finite (~600 msec; 33) and, thus, the effect on relaxivity due to the presence of water exchange across the intra- and extracellular compartment may need to be taken account. If in vitro and in vivo relaxivity were different, a slight error in the quantitative estimate of the in vivo [Mn^{++}] is expected. An independent histological/chemical analysis to quantify Mn^{++} in excised tissue will yield true tissue [Mn^{++}] and can be used to determine whether the relaxivity in vivo is significantly different from in vitro. Similarly, in principle, changes in T_1 values associated with forepaw stimulation is a quantitative indicator of neuronal synaptic activity as measured by intracellular Mn^{++} accumulation. If basal synaptic activity could be taken into account, quantitative synaptic activity associated with the forepaw stimulation could be obtained. T_1 of the neighboring contralateral cortex could be used to reflect basal Mn^{++} influx, assuming that the neigh-

Table 4
Center-of-Mass Spatial Offsets (in Unit of mm) Between Synaptic (T_1) and BOLD Activation Map, Between Synaptic and CBF Activation Map, and Between BOLD and CBF Activation Map[a]

	BOLD − T_1		CBF − T_1		BOLD − CBF	
	Δx[b]	Δy[c]	Δx[b]	Δy[c]	Δx[b]	Δy[c]
Rat 1	−0.87	−0.05	−0.66	−0.05	−0.21	0.09
Rat 2	−0.26	0.28	−0.07	0.26	−0.19	0.02
Rat 3	0.66	0.12	0.82	0.19	−0.16	−0.07
Rat 4	0.21	−0.07	0.45	−0.19	−0.23	0.12
Rat 5	−0.77	−0.23	−0.56	0.09	−0.21	−0.33
Rat 6	−0.07	−0.05	−0.14	0.05	0.07	−0.09
Rat 7	−0.19	0.40	−0.26	0.07	0.07	−0.14
Mean[d]	−0.18	−0.07	−0.06	0.06	−0.12	−0.06

[a]Δx and Δy are the distances between the center-of-mass of any two types of maps along the medial-lateral and dorsal-ventral direction, respectively.
[b]Negative sign indicates the center of mass of the first activation map is closer to the midline relative to that of the second activation map.
[c]Negative sign indicates the center of mass of the first activation map is closer to the dura relative to that of second activation map.
[d]The average COM offsets between activation maps are less than 200 μm, on the order of one pixel dimension (~230 μm).

boring contralateral cortex and the contralateral forepaw SI have similar level of basal synaptic activity and [Mn^{++}] delivered. Based on these assumptions, the estimated basal synaptic activity accounted for ~50% (~46 μM, Table 1) of the calcium activity under these experimental parameters. Alternatively, basal [Mn^{++}] influx can be obtained from a separate experiment in which Mn^{++} and mannitol are administered without forepaw stimulation or, similarly, mannitol can be simultaneously administered to both hemispheres while only one forepaw is stimulated.

In this study, we observed focal and marked T_1 reduction in the contralateral forepaw SI, consistent with the region expected to be responsive to forepaw stimulation based on autoradiographic, histological, and single-unit studies (26). Further, [Mn^{++}] in the contralateral SI was incrementally increased following each repeated stimulation epoch, indicating that the observed [Mn^{++}] change was specific to the forepaw stimulation. This selective Mn^{++} accumulation in the focal site was a result of increased synaptic activity and not the consequence of stimulus-induced CBF increase to the activated site (6). The observed T_1 decrease was predominantly the result of selective Mn^{++} accumulation in the intracellular, not the extracellular compartment (7–10, 34).

The highest level of activity ("hot spot") in the synaptic activity map was highly localized in the granular layer IV of the SI. This is consistent with the fact that layer IV, into which direct inputs from the thalamus are projected, is known to have the highest neuron density and exhibit the highest level of synaptic activity relative to the other cortical layers. On the other hand, results from Lin and Koretsky (5,6) and Aoki et al. (35) showed marked T_1-weighted contrast in the superficial cortical layer (around layers I and II) with minimal or comparable T_1-weighted contrast in the layer IV following forepaw stimulation. This discrepancy is likely due to the difference in the Mn^{++} infusion protocol. It appeared that the T_1-weighted contrast at the superficial layer predominantly arose from vascular Mn^{++} due to their continuous Mn^{++} infusion protocol. On the other hand, T_1 maps reported herein were taken at least 20–30 min after the termination of the Mn^{++} infusion. Consequently, with the intravascular half-life of ~4.7 min (36), the intravascular Mn^{++} contributions to the T_1 maps were minimal. Therefore, Mn^{++} infusion should be terminated to allow intravascular and extracellular Mn^{++} to dissipate before imaging synaptic activity such that unwanted vascular and extracellular signal contribution could be avoided. Based on these results, finding an optimal Mn^{++} dosage and imaging time window is critical in obtaining improved signal contrast and tissue spatial specificity.

Cross-Comparison of Hemodynamic Responses and Synaptic Activities

Cross-correlation coefficient is obtained by matching the experimental signal time course with the presented paradigm. It takes into account the signal change relative to the noise fluctuation and, thus, has statistical value (31). The CBF CC maps showed excellent spatial co-localization with synaptic activity maps and the region expected to be responsive to forepaw stimulation (26). This is consistent with the fact that the continuous arterial spin-labeling perfusion technique is primarily sensitive to microvasculature and tissues if sufficiently long labeling time is used. With the spin-labeling time of 3 sec, the stimulus-induced CBF increase will increase the number of labeled spins perfused into the tissue and/or capillaries (the mean transit time from the common carotid artery to the rat brain is ~200 msec; 37). On the other hand, the arterial signal contribution is minimal because the stimulus-induced CBF increase does not change the CBF contrast and there is also no physical (fluid) exchange with tissue at the arterial and arteriole level. Similarly, the venous signal contribution is also minimal because of the loss of inversion contrast by the time the labeled spins exit from the capillaries/tissues into the veins (i.e., no CBF contrast in the superior sagittal sinus was observed in background CBF images; see Fig. 3). Consequently, the CBF fMRI technique is expected to have relatively high spatial specificity (i.e., at the capillary/tissue level).

Similarly, BOLD statistical (CC) maps also showed excellent spatial co-localization with the synaptic activity maps, the CBF maps, and the region expected to be responsive to forepaw stimulation (26). This is consistent with the relatively high spatial specificity of the BOLD response at high magnetic field, where the extra- and intravascular (ΔR_2^*) BOLD effects from large vessels increase linearly with field strength, whereas the microvascular effect increases quadratically with magnetic field strength (38). Further, the T_2 and T_2^* of blood in large venous vessels are significantly shorter than those of tissue at high field. At 9.4 T, T_2 of blood is ~9 msec whereas that of brain tissue is ~40 msec (39). T_2^* of venous blood is expected to be even shorter. With the gradient echo time of 10 msec herein, the intravascular signals from large venous vessels to were markedly attenuated. Thus, BOLD statistical (CC) maps at high field is expected to yield excellent spatial co-localization with the CBF and synaptic activity maps. This appears not to be the case at low magnetic field as it had been demonstrated that the BOLD fMRI response at low field (≤1.5 T) arises predominantly from large vessels (40,41).

Interestingly, pixels with the highest BOLD percent change were localized to the cortical surface due to the extravascular contribution from superficial vessels. Thus, the percent-change BOLD maps obtained with gradient-echo technique did not correctly indicate the site/level of synaptic activity. This problem can be solved by using the spin-echo and/or flow-crushing gradient techniques (39) (though there is a significant loss of the BOLD contrast). On the other hand, regions with the highest CBF percent change were localized to the cortical layer IV and, thus, the percent-change CBF maps did correctly indicate the site/level of synaptic activity. This observation raises a very important question as to how pixels with large BOLD percent change should be interpreted if they have low statistical significance. For example, pixels containing predominantly large veins have low SNR due to short T_2^* of the venous blood and large signal fluctuation due to vasomotion. These pixels thus have large percent change but low statistical significance. Thus, statistical method should be used for functional localization and caution

must be exercised in interpreting BOLD percent change as an indicator for the level of neuronal activity. In this particular example, if large vessel contribution can be suppressed or eliminated, BOLD percent change is a good indicator for the level of neuronal activity.

Finally, it should be noted that there are some potential drawbacks associated with the method employed for cross-comparison herein. First, the T_1 images were acquired using two-segment SE EPI, whereas the BOLD and CBF images were acquired using single-shot GE EPI. This difference could result in different sensitivity toward image distortion primarily at the surface of the brain. However, if the GE BOLD technique yielded good spatial correspondence with synaptic activity, it is most likely that the SE BOLD would also yield good spatial correspondence because the SE technique is spatially more confined (39). Second, zero-filling the BOLD/CBF data matrix from 64×32 to 128×64 might yield registration errors on the order of one-half pixel between the synaptic activity and the BOLD/CBF maps. This has minor consequence because the conclusion of this study was that the overlaps among the three activation maps could be localized to within approximately one pixel dimension at best. Third, the 50-pixel criterion used in calculating the COM and spatial overlap could potentially be biased toward more spatial overlap. Because the CNR were different across the three different fMRI modalities, defining statistical thresholds of "equal" activation could not readily achieved. We thus chose a representative set of pixels ($\sim$50 pixels) that were most statistically significant such that comparisons could be made in a relatively robust manner across different modalities and different animals. Note that this criterion did not necessary force a good spatial correlation. For example, the COM of the percent-change BOLD maps (which has the highest percent change at the superficial layers; Fig. 3, third column) would have poor spatial correlation with those of the T_1 synaptic activity maps. Further, this criterion was only imposed on the calculations of the COM and the overlap maps. Other comparisons showed the raw data (i.e., Fig. 1C and D, and Fig. 3) without the imposed criterion and, thus, the degree of spatial localization across different activation maps can be visually assessed. In short, these minor drawbacks are very unlikely to alter the major conclusions of this study.

CONCLUSIONS

The spatial registration of the Mn^{++}-based synaptic activity technique showed excellent spatial co-localization with the commonly used BOLD and CBF fMRI techniques in the same animals. The stereotaxic coordinates obtained by the three fMRI modalities also showed excellent agreement with those obtained using the well-established techniques. These results strongly indicated that the Mn^{++} technique indeed measured calcium-dependent synaptic activity. One major implication of these results is that if macrovascular contributions can be minimized (i.e., with high field), hemodynamic-based fMRI techniques can be used to accurately map neuronal synaptic activities.

ACKNOWLEDGMENTS

The authors are in debt to Dr. Dae-Shik Kim for careful reading of the manuscript, Dr. Hellmut Merkle for maintenance of the MR scanner, and Mr. John Strupp for the STIMULATE software. The authors would also like to thank Prof. Alan Koretsky for providing a copy of Dr. Y.-J. Lin's thesis and Dr. Yi-Jen Lin for helpful suggestions.

REFERENCES

1. Nichollis JG, Martin AR, Wallace BG. Principles of synaptic transmission. In: From neuron to brain. Sinauer Associates; 1992. p 214–219, 299–300.
2. Kleinfeld D, Mitra PP, Helmchem F, Denk W. Fluctuations and stimulus-induced changes in blood flow observed in individual capillaries in layers 2 through 4 of the rat neocrotex. Proc Natl Acad Sci USA 1998;95:15741–15746.
3. Yuste R, Peinado A, Lawrence CK. Neuronal domains in developing neocortex. Science 1992;257:665–669.
4. Bear MF. Mechanism for a sliding synaptic modification threshold. Neuron 1995;15:1–4.
5. Lin Y-J, Koretsky AP. Manganese ion enhances T_1-weighted MRI during brain activation: an approach to direct imaging of brain function. Magn Reson Med 1997;38:378–398.
6. Lin Y-J. An approach to direct imaging of brain activation with MRI by activity-induced manganese dependent, "AIM," contras. Pittsburgh: Department of Biological Science, Carnegie Mellon University; 1997.
7. Drapeau P, Nachshen DA. Manganese fluxes and manganese-dependent neurotransmitter release in presynaptic nerve endings isolated from rat brain. J Physiol 1984;348:493–510.
8. Meiri U, Rahamimoff R. Neuromuscular transmission: inhibition by manganese ions. Science 1972;176:308–309.
9. Hallam TJ, Rink TJ. Agonists stimulate divalent cation channels in the plasma membrane of human platelets. FEBS Lett 1985;186:175–179.
10. Nirita K, Kawasaki F, Kita H. Mn and Mg influxes through Ca channels of motor nerve terminals are prevented by verapamil in frogs. Brain Res 1990;510:289–295.
11. Cotzias G, Horiuchi M, Fuenzalida S, Mena I. Clearance of tissue manganese concentrations with persistence of the neurological picture. Neurology 1968;18:376–382.
12. Newland M, Cox C, Hamada R, Oberdoerster G, Weiss R. The clearance of manganese chloride in the primate. Fundam Appl Toxicol 1987;9: 314–328.
13. Ogawa S, Lee T-M, Kay AR, Tank DW. Brain Magnetic Resonance Imaging with Contrast Dependent on Blood Oxygenation. Proc Natl Acad Sci USA 1990;87:9868–9872.
14. Detre JA, Leigh JS, Williams DS, Koretsky AP. Perfusion imaging. Magn Reson Med 1992;23:37–45.
15. Ueki M, Linn F, Hossmann K-A. Functional activation of cerebral blood flow and metabolism before and after global ischemia of rat brain. J Cereb Blood Flow Metab 1988;8:486–494.
16. Hyder F, Behar K, Martin M, Blamire A, Shulman R. Dynamic magnetic resonance imaging of the rat brain during forepaw stimulation. J Cereb Blood Flow Metab 1994;14:649–655.
17. Gyngell ML, Bock C, Schmitz B, Hoehn-Berlage M, Hossmann K-A. Variation of functional MRI signal response to frequency of somatosensory stimulation in α-chloralose anesthetized rats. Magn Reson Med 1996;36:13–15.
18. Kerskens CM, Hoehn-Berlage M, Schmitz B, Busch E, Bock C, Gyngell ML, Hossman K-A. Ultrafast perfusion-weighted MRI of functional brain activation in rats during forepaw stimulation: comparison with T_2^*-weighted MRI. NMR Biomed 1996;9:20–23.
19. Silva A, Lee S-P, Yang C, Iadecola C, Kim S-G. Simultaneous BOLD and perfusion functional MRI during forepaw stimulation in rats. J Cereb Blood Flow Metab 1999;19:871–879.
20. Silva AC, Lee S-P, Iadecola C, Kim S-G. Early temporal characteristics of CBF and deoxyhemoglobin changes during somatosensory stimulation. J Cereb Blood Flow Metab 2000;20:201–206.
21. Schupp DG, Merkle H, Ellermann JM, Ke Y, Garwood M. Localized detection of glioma glycolysis using edited 1H MRS. Magn Reson Med 1993;30:18–27.
22. Strupp JP. Stimulate: a GUI based fMRI analysis software package. NeuroImage 1996;3:S607.
23. Kim S-G, Hu X, Ugurbil K. Accurate T_1 determination from inversion recovery images: application to human brain at 4 tesla. Magn Reson Med 1994;31:445–449.

24. Riddle DR, Purves D. Individual variation and lateral asymmetry of the rat primary somatosensory cortex. J Neurosc 1995;15:4184–4195.
25. Narayan SM, Esfahani P, Blood AJ, Sikkens L, Toga AW. Functional increases in cerebral blood volume over somatosensory cortex. J Cereb Blood Flow Metab 1995;15:754–765.
26. Paxinos G, Watson C. The rat brain in stereotaxic coordinates. San Diego: Academic Press; 1986.
27. Silva AC, Zhang W, Williams DS, Koretsky AP. Estimation of water extraction fractions in rat brain using magnetic resonance measurement of perfusion with arterial spin labeling. Magn Reson Med 1997;37:58–68.
28. Herscovitch P, Raichle ME. What is the correct value for the brain-blood partition coefficient for water? J Cereb Blood Flow Metab 1985; 5:65–69.
29. Tsekos NV, Zhang F, Merkle H, Nagayama M, Iadecola C, Kim S-G. Quantitative measurements of cerebral blood flow in rats using the FAIR technique: correlation with previous iodoantipyrine autoradiographic studies. Magn Reson Med 1998;39:564–573.
30. Xiong J, Gao JH, Lancaster JL, Fox PT. Clustered pixels analysis for functional MRI activation studies of the human brain. Hum Brain Mapping 1995;3:287–301.
31. Chen W, Kato T, Zhu X-H, Strupp J, Ogawa S, Ugurbil K. Mapping of lateral geniculate nucleus activation during visual stimulation in human brain using fMRI. Magn Reson Med 1998;39:89–96.
32. Low W, Brawarnick N, Rahamimoff H. The inhibitory effect of Mn2+ on the ATP-dependent Ca2+ pump in rat brain synaptic plasma membrane vesicles. Biochem Pharmacol 1991;42:1537–1543.
33. Duong TQ, Springer CS, Sotak CH, Bretthorst GL, Vetek G, Palyka I, Ackerman JJH, Neil JJ. Evaluation of equilibrium transcytolemmal water exchange in intact rat brain. In: Proceedings of the ISMRM, Sydney, Australia, 1998. p 208.
34. Pautler R, Silva A, Koretsky A. In vivo neuronal tract tracing using manganese-enhanced magnetic resonance imaging. Magn Reson Med 1998;40:740–748.
35. Aoki I, Tanaka C, Takegami T, Ebisu T, Umeda M, Fukunaga M, Someya Y, Watanabe Y. Experimental functional MRI using dynamic activity-induced manganese dependent contrast (DAIM). In: Proceedings of the ISMRM, Philadelphia, 1999. p 359.
36. Gerdin B, Mccann E, Lunderg C, Arfors K-E. Selective tissue accumulation of manganese and its effect on regional blood flow and haemodynamics after intravenous infusion of its chloride salt in the rat. Int J Tissue React 1985;7:373–380.
37. Zhang W, Williams DS, Detre JA, Koretsky AP. Measurement of brain perfusion by volume-localized NMR spectroscopy using inversion of arterial water spins: accounting for transit time and cross-relaxation. Magn Reson Med 1992;25:362–371.
38. Ogawa S, Menon RS, Tank DW, Kim S-G, Merkle H, Ellermann JM, Ugurbil K. Functional brain mapping by blood oxygenation level-dependent contrast magnetic resonance imaging. Biophys J 1993;64:800–812.
39. Lee S-P, Silva AC, Ugurbil K, Kim S-G. Diffusion-weighted spin-echo fMRI at 9.4 T: microvasculuar/tissue contribution to BOLD signal change. Magn Reson Med 1999;42:919–928.
40. Song AW, Wong EC, Jezmanowicz A, Tan SG, Hyde JS. Diffusion weighted fMRI at 1.5T and 3T. In: Proceedings of the 3rd Scientific Meeting of SMRM, Nice, France, 1995. p 457.
41. Song AW, Wong EC, Tan SG, Hyde JS. Diffusion-weighted fMRI at 1.5T. Magn Reson Med 1996;35:155–158.